Structural response of an atomically-precise silver nanocluster to solvent interactions

Daniel M. Chevrier,^{1,†} Brian E. Conn,² Bo Li,³ De-en Jiang,³ Terry Bigioni,² Amares Chatt,¹ Peng Zhang*¹

¹Department of Chemistry, Dalhousie University, Halifax, NS B3H 4J3, Canada

²Department of Chemistry and Biochemistry, University of Toledo, Toledo, Ohio 43606, United States

³Department of Chemistry, University of California, Riverside, California 92521, United States

KEYWORDS: Metal nanocluster, Thiolate-silver, XAFS, QM/MM, Local structure, Solvent interactions, Coordinating solvents

ABSTRACT: Atomically-precise metal nanoclusters exhibit robust electronic, chemical and optical properties and have compositions that can be described with an exact number of metal atoms and protecting ligands, i.e. they are molecules, making them ideal systems to uncover nanoscale structure-property relationships. Recently, silver nanoclusters have garnered considerable attention after the high-yield synthesis and crystallization of a stable thiolate-protected silver nanocluster, M₄Ag₄₄(SR)₃₀ (M – counter-cation; SR – protecting thiolate ligand). The structure of M₄Ag₄₄(SR)₃₀ has a distinct clusterin-cluster Ag core (Ag₁₂+Ag₂₀) that is protected with six isometric capping units (Ag₂(SR)₅). Interestingly, the ligand shell has solvent accessible regions due to the bundling of protecting ligands. Despite the exposed nature of the surface, the cluster has demonstrated outstanding stability and resistance to chemical reaction. Herein, we investigate the interaction of coordinating solvents with the M₄Ag₄₄(SR)₃₀ nanocluster core, surface and ligand shell and propose that coordinating solvents and semi-aqueous conditions play an important role in protecting exposed surface regions and can further influence the local structure of the silver nanocluster itself. Through XAFS and quantum mechanical/molecular mechanical studies of Na₄Ag₄₄(p-MBA)₃₀ (p-MBA - para-mercaptobenzenoic acid), we found that strongly coordinating aprotic solvents such as DMF and DMSO interact with surface Ag atoms particularly between ligand bundles to compress the Ag core and relax surface Ag-S interactions. Under semi-aqueous conditions, aprotic coordinating solvent molecules preferentially remain on the metal surface while water molecules interact with ligands. Ligand bundling persisted across the tested solvation conditions. This work demonstrates that M₄Ag₄₄(SR)₃₀ nanoclusters are sensitive to solvent interactions, indicating that the choice of solvent can influence stability and possibly formation of these highly stable silver nanoclusters. Moreover, solventnanocluster interactions should be carefully considered moving forward for silver nanoclusters, particularly with ligand bundles, as they can influence the electronic/chemical properties of the nanocluster as well as the surface accessibility of small molecules for catalysis-based applications.

Thiolate-protected silver nanoparticles (Ag NPs) and smaller (1-3 nm diameter) nanoclusters (Ag NCs) have been investigated for several years alongside the groundbreaking progress made with thiolate-protected Au NPs and NCs.¹⁻⁴ After the gigantic leap forward in elucidating thiolate-protected Au NC structure and properties (i.e., crystallization of Au₁₀₂)⁵, progress in Ag NC analogs soon followed. Ag-based NPs and NCs are an enticing alternative since Ag is not as precious as Au and offers another suite of chemical and physical properties employable for application. For example, the antibacterial properties of Ag can be utilized for biomedical applications⁶ and the superior optical properties of Ag-based NPs have shown potential as advanced light harvesting materials.7 Importantly, the lower cost of Ag is beneficial for scaling up syntheses toward cost-effective production for application or industrial

utilization. Despite these advantages, Ag NPs have been known to suffer from tarnishing,⁸ which affects Ag NP stability and long-term usage of these materials in application stages or on an industrial scale. This also interferes with the fundamental characterization and understanding of optical and electronic properties as they relate to size, structure and surface environment of nano Ag.

More recently, thiolate-protected Ag NCs have made significant progress in the field of atomically-precise clusters. Advances in metal NC synthesis techniques have enabled the preparation and isolation of new Ag species, but only a few new Ag_n(SR)_m NCs (where n and m are integers, and SR is the protecting thiolate ligand) have known structures.^{9,10} Notably, structural elucidation of M₄Ag₄₄(SR)₃₀ NCs was a significant discovery for the metal NC communi-

ty. 11,12 The crystal structures revealed a distinctive metal core with discrete Ag-SR surface structural units, much like the general construction of thiolate-protected Au NCs. The exceptional stability of M₄Ag₄₄(SR)₃₀ is unprecedented for Ag NPs and NCs, however. 12 The M₄Ag₄₄(SR)₃₀ structure is so greatly favoured over other Ag structures that single-species M₄Ag₄₄(SR)₃₀ products are attainable in quantitative yields, and the reaction can be scaled up to produce over 100 g of M₄Ag₄₄(SR)₃₀ NCs per batch. 12,13 Other properties of interest for M₄Ag₄₄(SR)₃₀ NCs include a rich, broadband light absorption across the UV-Vis spectrum, moderate PL emission, and catalytic activity. 13,14,TPB1

The exceptional stability of $M_4Ag_{44}(SR)_{30}$ has been attributed to the closed atomic shell structure of the Ag_{32} core (Ag_{12} icosahedron inside Ag_{20} dodecahedron), the closed electronic shell structure of the molecule ($1S^2|1P^6|1D^{10}$, following the Aufbau rule), and the choice of protecting ligands. It was also recognized that coordinating solvents played a key role in the stabilization of $M_4Ag_{44}(pMBA)_{30}$, although the mechanism of protection was not understood. Further, it was demonstrated that increasing the coordination strength of the solvent during synthesis increased the yield of $M_4Ag_{44}(pMBA)_{30}$ NCs. 13

Ligand shells are often thought of as isotropic coatings that offer uniform protection, however this is generally not the case. Intramolecular interactions between ligands in the protective outer shell are known to result in the bundling of ligands, which can impart more complex structure to the ligand shell. TPB2, TPB3 In the case of Na₄Ag₄₄(p-MBA)₃₀, the p-MBA ligands were observed to form dimer and trimer bundles through π - π (face-to-face) and C-H--- π (edge-to-face) interactions between benzene rings, respectively, in the x-ray determined crystal structure. Surprisingly, ligand bundling was also observed in NMR measurements of fully solvated molecules, suggesting that these intramolecular interactions are strong enough for the gaps in the ligand shell structure to persist in solution. 13

It has been recognized that the gaps created by ligand bundling in Na₄Ag₄₄(pMBA)₃₀ leave some of the Ag atoms unprotected and consequently exposed to potential chemical attack. It was therefore postulated that the coordinating solvent molecules could be acting to protect the exposed Ag atoms, effectively forming a second shell of steric protection. Such a secondary protective layer was not directly observed in x-ray structure measurements, however, presumably due to the mobility of the coordinating solvent molecules within the solvent-containing cavities of Na₄Ag₄₄(pMBA)₃₀ crystals. It therefore remains an open question as to the role of coordinating solvent molecules and the nature of their interactions with surface structures in the stability of Na₄Ag₄₄(pMBA)₃₀, in particular, as well as other related NCs.

With ligand shell and surface-based interactions recently generating significant interest, $^{18-21}$ there is a growing need for more detailed information on solvent effects on metal NC structures and surface chemistry. Toward this end, the local structure of Ag44(SR)30 NCs was examined using XAFS and quantum mechanical/molecular mechanical (QM/MM)

to understand how coordinating solvent molecules interact and affect the ligand shell and structure of $M_4Ag_{44}(SR)_{30}$. We demonstrate that the response of $Na_4Ag_{44}(p\text{-MBA})_{30}$ NCs to solvation interactions is measurable and provides insight into how coordinating solvents stabilize the surface between ligand bundles and in turn affect the structure of $M_4Ag_{44}(SR)_{30}$. Furthermore, this work demonstrates the utility of XAFS techniques for examining the surface chemistry of atomically-precise metal NCs in solution.

MATERIALS AND METHODS

Na₄Ag₄₄(p-MBA)₃₀ NCs (p-MBA = para-mercaptobenzoic acid) were synthesized according to the protocol published by Desireddy $et\ al.^{12}$ Pertaining to this study, the reaction mixture used a water-DMSO co-solvent and the final product was precipitated using DMF.

Ag K-edge XAFS data was collected for Na₄Ag₄₄(p-MBA)₃₀ NC samples from the CLS@APS beamline (Sector 20-BM) at the Advanced Photon Source (operating at 7.0 GeV). Both solid- and solution-phase measurements were conducted at 300 K and atmospheric pressure. The powdered sample collected at 90 K for the initial multi-shell fitting analysis was loaded into a helium-cooled cryostat chamber for measurement. Na₄Ag₄₄(p-MBA)₃₀ NCs for solid-phase samples were prepared by dissolving clusters in a small amount of DMF or DMSO (20 mg of NCs in 100 uL solvent) and drop-casting them onto a Kapton film. The concentrated drops were left to dry under N₂ for at least one hour and then folded until an absorption of at least 0.5 was achieved. Solution-phase samples were prepared using a ~10 mM solution of Na₄Ag₄₄(p-MBA)₃₀ NCs and utilizing a Teflon liquid cell with Kapton windows (designed and constructed at the CLS@APS beamline).

The amplitude reduction factor (S_0^2) was fixed at 0.90 for Ag K-edge EXAFS fitting, which was determined by fitting the Ag-Ag scattering of a Ag foil reference with a fixed Ag-Ag coordination number (CN) of 12. For multi-shell EXAFS fitting, CNs were fixed according to the Na₄Ag₄₄(p-MBA)₃₀ crystal structure. Theoretical phase and scattering amplitudes for Ag-S and Ag-Ag scattering paths were calculated using the Na₄Ag₄₄(p-MBA)₃₀ crystal structure model. A krange of 3 to 12 Å-1 was used for the Fourier transformation to R-space. A fitting window of 1.5 to 3.5 Å was used for fits. Reported uncertainties for EXAFS fitting results were computed from off-diagonal elements of the correlation matrix, which were weighted by the square root of the reduced chi-squared value obtained from each simulated fit. The amount of experimental noise was also taken into consideration for each Fourier transformed Rspace spectrum from 15–25 Å.²² S K-edge XANES data were collected from the SXRMB beamline at the Canadian Light Source (operating at 2.9 GeV). Powdered samples were measured in fluorescence mode under room temperature and vacuum conditions. All samples were mounted onto a copper sample using carbon tape. Liquid-phase measurements were conducted in a fluorescence mode using a Teflon liquid cell with a mylar measurement window.

The QM/MM molecular dynamics (MD) simulations were performed to investigate the influence of the different

solvents on the structure of a Ag NC. The initial structure of [Ag₄₄(*p*-MBA)₃₀]⁴⁻ was taken from the X-ray crystallography data¹² and then solvated in two types of solvent environments: 1) pure solvent of 1514 DMSO molecules; 2) a co-solvent of 265 DMSO and 2651 water molecules. Four Na⁺ ions were added to balance the charge.

The solvated systems were simulated with periodic boundary conditions and were first equilibrated with classical MD (CMD) for 50 ns at constant number, pressure, and temperature (NPT ensemble), with T = 300 K, P = 1atm, and with the time step of 1 fs. We performed CMD simulations using the Amber 18 package²³ together with the GAFF,²⁴ FF14SB²⁵ and TIP3P²⁶ force-fields. The positions of the Ag atoms were fixed during CMD simulations since our goal was to equilibrate the solvation structure. The atomic charges in $[Ag_{44}(p-MBA)_{30}]^{4-}$ were derived from fitting the restrained electrostatic potential (RESP) using CP2K.²⁷ Representative snapshots of the solvated systems after pre-equilibration were then used in the QM/MM simulations. The energies of the QM region containing the $[Ag_{44}(p-MBA)_{30}]^{4-}$ cluster and the solvents in the first solvation shell were computed using the Quickstep module of CP2K, while the MM regions containing the remaining solvents were treated using the FIST module of CP2K with the same force field as in the CMD simulations. The QM regions were described with the mixed Gaussian and plane wave (GPW) approach using the Perdew-Burke-Ernzerhof (PBE) functional²⁸ and the MOLOPT basis set with a double-ζ Gaussian basis set augmented with a set of p-type polarization functions (DZVP).29 Plane waves were expanded up to a density cutoff of 400 Ry and used in conjunction with the GTH pseudopotentials to describe the core electrons.³⁰⁻³² The convergence threshold of the electronic structure relaxation was set to 10⁻⁶ Hartree. We also employed dispersion corrections in the OM calculations.³³ Six Gaussian functions were used for the Gaussian expansion of the electrostatic Potential (GEEP) to couple the QM and MM regions.34,35 The QM box was cubic with a cell length of 30 Å. The periodicity was only applied to the MM box with a cell length of 57 Å (pure DMSO) and 50 Å (water-DMSO) and the QM images were decoupled using the wavelet scheme.36,37 The QM/MM simulations were carried out in NVT ensemble at 300 K for about 15 ps, with the last half of the trajectories being used for analysis.

RESULTS AND DISCUSSION

Separately probing the core and surface bonding environments of $Na_4Ag_{44}(p\text{-}MBA)_{30}$

The crystal structure of Na₄Ag₄4(p-MBA)₃₀ (Figure 1a) has a compact Ag₃₂ core that is composed of a hollow Ag₁₂ icosahedron inside of a Ag₂₀ dodecahedron. Protecting the Ag₃₂ core are six Ag₂(p-MBA)₅ capping units known as "mount" motifs (or mounts), which are positioned in an octahedral geometry around the Ag₃₂ core. Bundles of two and three ligands can be seen on each mount, which result from the intramolecular π - π interactions between p-MBA ligands (Figure 1b). This organization of the ligands exposes the 12 Ag atoms in the 6 mounts as well as 8 Ag atoms at

the feet of the mounts in the dodecahedral shell, which together form a cube. $^{\text{TPB3}}$

From inspection of the Ag-Ag and Ag-S bond length distributions in the crystal structure (Figure 1c), three distinct environments were identified as EXAFS scattering shells for fitting analysis. The Ag-S shell corresponds to covalent bonding between thiolate ligands and Ag sites in the Ag20 cage and in the mounts (Figure 1a, top right). The shorter distance Ag-Ag shell (Ag-Ag1) corresponds to bonding within the hollow Ag12 icosahedron as well as bonding between Ag12 and the Ag20 cage (Figure 1a). The third shell, Ag-Ag2, represents Ag-Ag bonding at a longer distance, namely between the two Ag atoms in the mounts, between Ag atoms within the Ag20 cage, and between mount and cage Ag sites.

Ag K-edge EXAFS of Na₄Ag₄₄(p-MBA)₃₀ in the solid-phase at 90 K was first analyzed using the Ag-S and Ag-Ag scattering shells described above; the fit is shown in Figure 1d and fitted parameters are given in Table 1. Fitted Ag-S and Ag-Ag bond distances matched well with the average bond lengths calculated from the crystal structure ($R_{Ag-S} = 2.55$ Å, $R_{Ag-Ag1} = 2.84$ Å, $R_{Ag-Ag2} = 3.14$ Å), verifying the suitability of the designated scattering shells to account for, and distinguish, core and surface interactions.

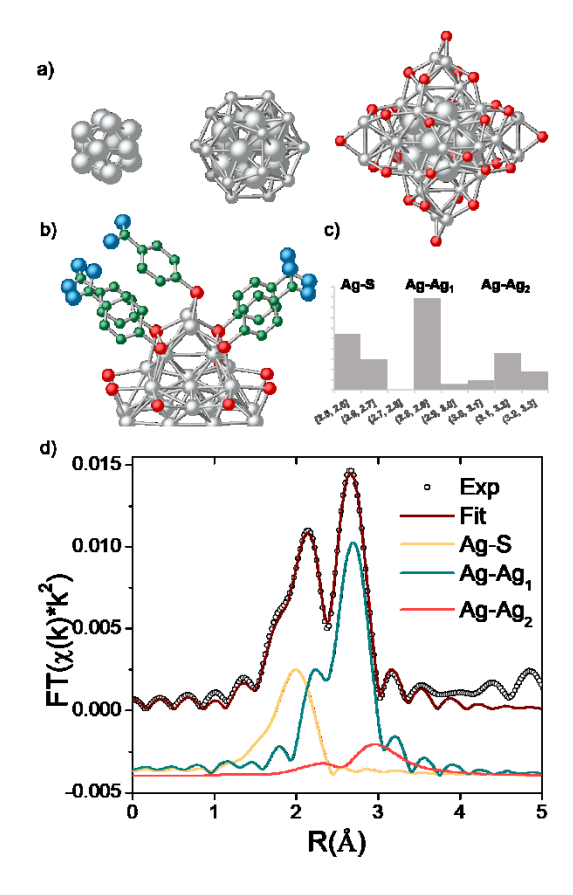


Figure 1. a) Na₄Ag₄₄(p-MBA)₃₀ structure from center to surface: hollow icosahedron (Ag₁₂) to Ag₂₀ dodecahedron to six Ag₂S₅ mounts (silver – Ag, red – S). The organic portion of the protecting ligands are removed for clarity. b) Mount structures on the surface of Na₄Ag₄₄(p-MBA)₃₀ clus-

ters (blue – 0, green – C) illustrating ligand bundling and open clefts. c) Bond length distribution histogram of Na₄Ag₄₄(p-MBA)₃₀ with assigned EXAFS scattering paths. d) Ag K-edge R-space of Na₄Ag₄₄(p-MBA)₃₀ NCs at 90 K in the solid-phase, showing total fit and individual contributions from each scattering path.

Solid- and solution-phase XAFS measurements were conducted at 300 K for Na₄Ag₄₄(p-MBA)₃₀ NCs (k-space spectra shown in Figure S1). The EXAFS spectra were fitted for each condition using the three scattering shells described and are shown in Figure S2, with associated fitting results in Table 2. We note that the near-edge structure (Figure S3) varies little across the series of Na₄Ag₄₄(p-MBA)₃₀ measurements in various conditions, which is due to the fully occupied final valence states in the dipole-allowed transition from 1s \rightarrow 4p for Ag K.

EXAFS fitting results for $Na_4Ag_{44}(p\text{-MBA})_{30}$ at 300 K in the solid-phase were consistent with results from 90 K, but with small variations in average bond distances and as expected higher Debye-Waller factors from thermal disorder. Notably, Ag-S and surface Ag-Ag (Ag-Ag₂) bond distances did not change significantly with temperature whereas Ag-Ag bonds related to the Ag_{12} core decreased in length. The solid-phase temperature comparison may demonstrate a rigid surface layer while the hollow Ag_{12} core is more susceptible to thermal vibrations and fluctuations.

Table 1. EXAFS fitting results for Na₄Ag₄₄(p-MBA)₃₀ at 90 K in the solid-phase. Uncertainties in fitted parameters are shown in parentheses; Debye-Waller factor (σ^2); energy-shift parameter, ΔE_0 .

		-	•	
Shell	CN	R (Å)	σ^2 (Å ²)	ΔE_0 (eV)
Ag-S	1.9	2.501(7)	0.0066(4)	1(1)
Ag-Ag ₁	4.1	2.876(3)	0.0051(1)	2.0(4)
Ag-Ag ₂	3.3	3.08(1)	0.021(3)	2.0(4)

Coordinating aprotic solvent molecules interact directly with nanocluster surface

Solvents for examining the effects of solvation (DMSO, DMF and water) were selected based on the documented preparation of Na₄Ag₄₄(p-MBA)₃₀ NCs.¹² Solution-phase studies were first conducted with coordinating aprotic solvents DMSO and DMF. Na₄Ag₄₄(p-MBA)₃₀ NCs in DMF or DMSO had similar structural responses to solvation when comparing the fitted parameters with the solid-phase EXAFS measurements (fitting results in Table 2). The average Ag-S bond length increased by \sim 0.02 Å when dissolved in DMF or DMSO and the associated Debye-Waller factor remained similar to the solid phase. Exterior Ag-Ag interactions (Ag-Ag₂) markedly decreased in average distance for Na₄Ag₄₄(p-MBA)₃₀ in solution, while the interior Ag-Ag bonding within the Ag₃₂ core (Ag-Ag₁) decreased only slightly in distance and disorder.

Table 2. EXAFS fitting results for Na₄Ag₄₄(p-MBA)₃₀ NCs in solid-phase and in various solution-phase conditions at 300 K. Uncertainties in fitted parameter are shown in parentheses; Debye–Waller factor (σ^2); energy-shift parameter, ΔE_0 .

85 P	, —	-0-		
Condition	Shell	R (Å)	σ^2 (Å ²)	ΔE_0 (eV)
	Ag-S	2.50(1)	0.011(1)	0(1)
Solid	Ag-Ag ₁	2.83(1)	0.013(1)	0(1)
	Ag-Ag ₂	3.09(5)	0.03(1)	0(1)
	Ag-S	2.525(7)	0.010(6)	-2.0(6)
DMF	Ag-Ag ₁	2.816(5)	0.011(4)	-2.0(6)
	Ag-Ag ₂	3.02(2)	0.031(6)	-2.0(6)
	Ag-S	2.52(1)	0.010(9)	-1.4(8)
DMSO	Ag-Ag ₁	2.818(8)	0.012(7)	-1.4(8)
	Ag-Ag ₂	3.04(3)	0.025(6)	-1.4(8)
	Ag-S	2.49(1)	0.0083(6)	-3(1)
25% DMSO	Ag-Ag ₁	2.863(8)	0.0123(7)	1.7(9)
	Ag-Ag ₂	3.07(2)	0.023(4)	1.7(9)
100/	Ag-S	2.479(9)	0.0097(4)	-2(1)
10% DMSO	Ag-Ag ₁	2.854(5)	0.0114(4)	2.1(5)
	Ag-Ag ₂	3.05(1)	0.020(2)	2.1(5)

Measurements of the S K-edge absorption (Figure S4) provide a complementary perspective and reveal that the electronic properties of the S atoms change when in solution (only DMF was measured since the S within DMSO interferes with this measurement). The white-line for Na₄Ag₄₄(p-MBA)₃₀ was broadened compared to free thiol ligands is due to S-Ag interactions. The white-line intensity for Na₄Ag₄₄(p-MBA)₃₀ was higher in DMF than in the solid-phase, which could be due to redistribution of electron orbital density in S as a result of solvent interactions with the p-MBA ligands or Ag NC core. This shift in electron density from the S atoms to the Ag NC core would be consistent with core contraction under solvation.

Disappearance of the pre-edge feature for Na₄Ag₄₄(p-MBA)₃₀ upon dissolution of the solid into DMF is interesting to note. The origin of this feature is typically due to spin-forbidden quadrupole 1s \rightarrow 3d transitions for S and has been observed to be more prominent with the higher contribution of metal-metal bonding, but also when there are vacancies in the LUMO states for the bound metal species.^{38,39} Since there is no compositional change of Na₄Ag₄₄(p-MBA)₃₀ in solution the change in electronic properties of S could be due to small changes in the Ag-S-C bond, where variable bond angles and orientations could

broaden the observed solid-phase transition. However, as observed by NMR and as will be seen from QM/MM simulations, ligand bundles are not entirely disrupted by solvation. A more likely explanation could be changes in S and/or Ag atom electron density due to coordinating solvent interactions.

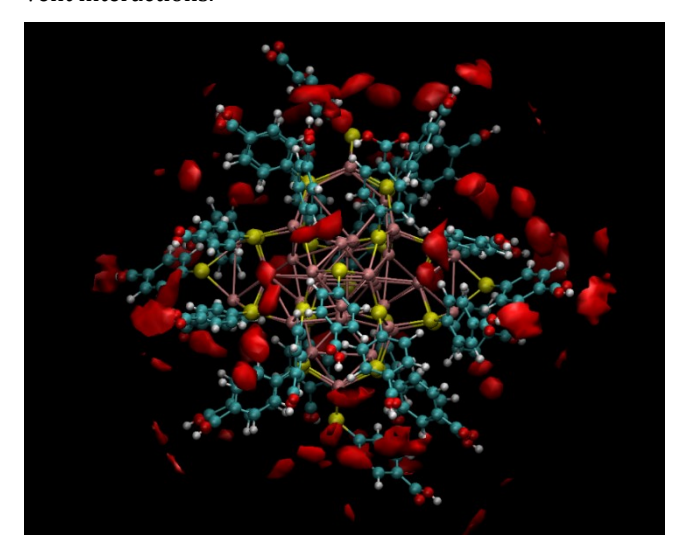


Figure 2. QM/MM simulations of DMSO (red clouds) distribution around $Na_4Ag_{44}(p\text{-MBA})_{30}$ (pink – Ag, yellow – S, cyan – C, red – O, white - H).

To pinpoint and further confirm the contracting Ag framework and the potential change in electronic properties of S and Ag, QM/MM simulations were conducted on a Na₄Ag₄₄(p-MBA)₃₀ cluster surrounded by DMSO molecules. QM treatment was given to the Na₄Ag₄₄(p-MBA)₃₀ cluster and its first solvation shell while MM was used for the surrounding solvent environment. It can be seen from a simulation with DMSO molecules in Figure 2 that the coordinating solvent occupies regions between ligand bundles, from the carboxylic acid ends of p-MBA to the Ag NC surface. The closest average radial distance of the coordinating sulfoxide residue to the Ag atoms on the surface was found to be \sim 3.0 Å (Figure S5a), which is short enough for considerable electronic interactions. The sulfoxide residue distance to S atoms is on average slightly longer at ~4.0 Å (Figure S5b). Together, these results indicate that the positions of the DMSO molecules were not entirely random, with a preference for positions nearer the Ag atoms. Relating the proximity of DMSO molecules to the Ag NC surface to the experimental result of contracted Ag core and the change in S electronic properties, it is evident that an electronic interaction between the solvent and the Ag NC surface could account for these observations.

Compared to our previous EXAFS studies of Au_n(SR)_m NCs in solution, less surface structural disorder was measured for Na₄Ag₄₄(*p*-MBA)₃₀ NCs in solution. The observation of solution-phase ligand bundling on Na₄Ag₄₄(*p*-MBA)₃₀ NCs by NMR as well as by QM/MM simulations suggests that ligand-ligand interactions are strong enough to enable ligand bundling to persist in dynamic environments. This solution-phase bundling creates opportunities for significant interactions between solvent molecules and Ag atoms on the surface, rather than only solvent-ligand interac-

tions. The carboxylic acid groups may also play a role in ligand bundling and may interact with water molecules through hydrogen bonding to further stabilize ligand bundles. Based on the solution-induced changes of Ag-S and Ag-Ag bonding measured by EXAFS, the solution-phase p-MBA ligand bundling observed by NMR and QM/MM simulations, and the requirement of coordinating solvents in the synthesis of Na₄Ag₄₄(p-MBA)₃₀ NCs, the coordination interaction of DMSO and DMF solvents are hypothesized to play an important role in the overall stability of the NC.

Water as a co-solvent interacts with ligands and surface, relaxing Ag NC core

The final consideration is how water molecules combine with aprotic solvent molecules to influence the core and surface environment of Na₄Ag₄₄(p-MBA)₃₀ NCs. Based on the semi-aqueous reaction conditions and our initial observation of DMSO interacting with the Ag NC surface, we tested the structural response of Na₄Ag₄₄(p-MBA)₃₀ to solution-phase conditions where water was added as a cosolvent. Two solvent mixtures of DMSO (coordinating with the Ag NC surface) and water (interacting with carboxylate groups) were tested: 25% (v/v) DMSO/H₂O and 10% (v/v) DMSO/H₂O. Below 10% (v/v) DMSO, solutions were no longer stable enough for XAFS measurement.

Interestingly, both solvent mixtures had similar EXAFS fitting results. Compared to pure DMSO, the Ag-S bonds shortened by up to $\sim\!0.04$ Å and the metallic Ag-Ag bonds in the Ag12 inner shell (Ag-Ag1) were longer than in pure DMSO. No increase in surface or core bond disorder was detected for Ag-Ag interactions based on the fitted Debye-Waller factors, in fact a small decrease was observed. The fitting uncertainty associated with the Debye-Waller factor for Ag-S distances decreased from 90% to 4-7% when going from DMSO to DMSO/H2O solvents. The change in the Ag-S bond length and this reduction in fitting uncertainty suggest that the combination of aprotic and protic solvents could be working together to stabilize the Ag NC surface and ligand shell, respectively.

These two possible modes of solvation were further studied using QM/MM simulations. In these simulations, water molecules (less coordinating than DMSO) were expected to interact with the carboxylic acid groups on *p*-MBA through hydrogen-bonding (bringing together ligand bundles and reducing intermolecular rotations) while DMSO molecules were expected to interact with the Ag NC surface in the clefts between ligand bundles (similar to pure DMSO).

As anticipated, when the DMSO concentration was 10% in our QM/MM simulation, DMSO molecules were mainly found in surface cleft regions whereas water molecules were found at all locations on the surface of Na₄Ag₄₄(p-MBA)₃₀, indicating a favourable interaction between DMSO and surface Ag atoms. The radial distribution plot of distances between DMSO oxygen atoms and surface Ag atoms consists of only one strong peak at a distance of \sim 3 Å, as shown in Figure S5. This indicates both that DMSO selectively partitions to the surface of Na₄Ag₄₄(p-MBA)₃₀ and that the oxygen atoms are the coordinating residue, given the strong orientation preference. The first peak was also

shifted by \sim 0.2 Å as well as significantly broadened, which is consistent with the low DMSO concentration and the transient nature of solvent coordination. The absence of a second solvation shell is consistent with the low DMSO concentration and with the absence of a strong preferential interaction between first and second DMSO solvation shells.

The QM/MM simulations were also able to provide information on the response of the $Na_4Ag_{44}(p\text{-}MBA)_{30}$ structure to solvent coordination. From these simulation results, we found that $Ag\text{-}Ag_1$ bonding decreased on average by $\sim\!0.04$ Å (Figure S5) when the amount of coordinating DMSO was increased from 10% to 100%. This is consistent with our EXAFS results (Table 2) and further supports our findings on the effects of solvent coordination.

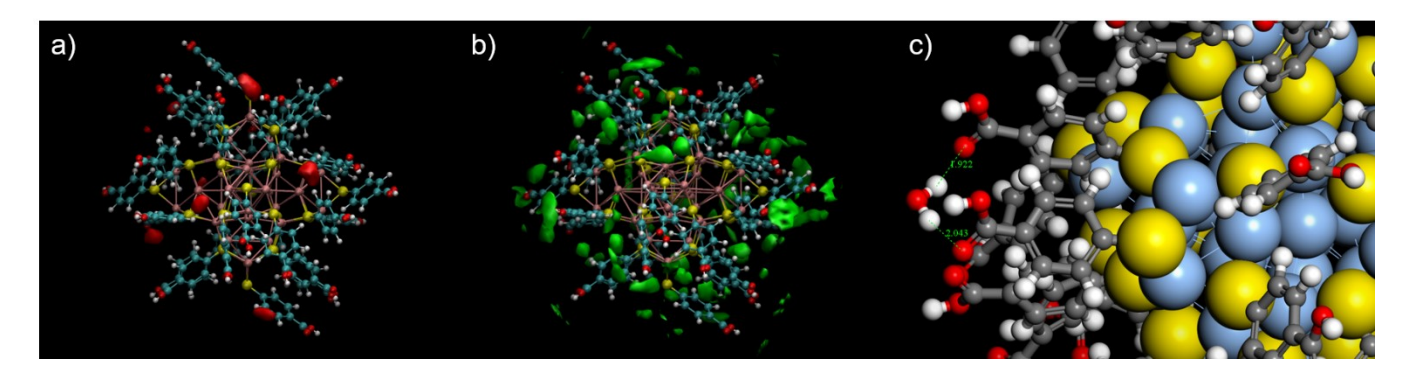


Figure 3. QM/MM simulations showing the distribution of a) DMSO (red cloud) and b) H_2O (green cloud) around $Na_4Ag_{44}(p-MBA)_{30}$ in 10% DMSO and 90% H_2O (pink – Ag, yellow – S, cyan – C, red – O, white - H). c) Interactions between water molecules and carboxylate residues from QM/MM simulations.

CONCLUSION

Solution-phase XAFS and QM/MM simulations were employed to investigate solvation coordination and its influence on the structure of Na₄Ag₄₄(p-MBA)₃₀ as well as its remarkable stability. From EXAFS measurements and analysis, core and surface bonding environments were individually monitored with EXAFS fitting analysis and showed structural changes that correlated with solvent coordination. These results indicate that strongly coordinating molecules such as DMSO and DMF directly interact with Ag atoms on the surface of Na₄Ag₄₄(p-MBA)₃₀ and lead to contraction of the Ag₁₂ inner core. In addition, Ag-S distances were observed to increase due to the coordinating solvent molecules. QM/MM simulations found that DMSO coordinated with Na₄Ag₄₄(p-MBA)₃₀ via its O atom and was preferentially located on the Ag surface between the bundles, which could provide a secondary mechanism of steric stabilization. This work demonstrates the chemical effect of coordinating solvents on Na₄Ag₄₄(p-MBA)₃₀ NCs, strongly supporting its critical role in the exceptional stability of Na₄Ag₄₄(p-MBA)₃₀. This work paves the way for the development of entirely new synthetic strategies where the choice of solvent type may also influence the surface accessibility, the electronic properties, and ultimately the stability of metal NCs, particularly for less inert metals. This could play an important role in the development of new NC technologies, such as Ag NC $\,$ sensors and catalysts.

ASSOCIATED CONTENT

Supporting Information. Ag K-edge XAFS data for all samples presented in k-space, Fourier transformed R-space with fitted scattering paths and XANES spectra. S K-edge XANES for solid phase and solution phase comparison. Radial distribution plots for various interaction distances between sulfoxide residues, Ag atoms and thiolate S atoms. This material is available free of charge via the Internet at http://pubs.acs.org.

AUTHOR INFORMATION

Corresponding Author

* peng.zhang@dal.ca

Present Addresses

† Biosciences and Biotechnologies Institute of Aix-Marseille, CEA Cadarache, 13108 St. Paul lez Durance, France

Author Contributions

The manuscript was written through contributions of all authors. / All authors have given approval to the final version of the manuscript.

Funding Sources

TPB thanks the National Science Foundation for financial support (grants #0955148 and #1905262).

ACKNOWLEDGMENT

D.M.C. would like to thank NSERC for financial support through the Alexander Graham Bell Canada Graduate Scholarship during the time this research was conducted.

B.E.C. would like to thank the IPMI for financial support through an IPMI graduate fellowship.

ABBREVIATIONS

NP, nanoparticle; NC, nanocluster; XAFS, X-ray absorption fine structure; EXAFS, extended X-ray absorption fine structure; XANES, X-ray absorption near-edge structure; QM/MM, quantum mechanics / molecular mechanics; SR, thiolate; DMSO, dimethylsulfoxide; DMF, dimethylformamide; *p*-MBA, *para*-mercaptobenzenoic acid

REFERENCES

- (1) Jain, P. K.; Huang, X.; El-Sayed, I. H.; El-Sayed, M. A. Noble Metals on the Nanoscale: Optical and Photothermal Properties and Some Applications in Imaging, Sensing, Biology, and Medicine. Acc. Chem. Res. 2008, 41 (12), 1578– 1586.
- (2) Kang, S. Y.; Kim, K. Comparative Study of Dodecanethiol-Derivatized Silver Nanoparticles Prepared in One-Phase and Two-Phase Systems. *Langmuir* 1998, 14, 226–230.
- (3) Kumar, S.; Bolan, M. D.; Bigioni, T. P. Glutathione-Stabilized Magic-Number Silver Cluster Compounds. J. Am. Chem. Soc. 2010, 132 (38), 13141–13143.
- (4) He, S.; Yao, J.; Jiang, P.; Shi, D.; Zhang, H.; Xie, S.; Pang, S.; Gao, H. Formation of Silver Nanoparticles and Self-Assembled Two-Dimensional Ordered Superlattice. *Langmuir* 2001, 17 (5), 1571–1575.
- (5) Jadzinsky, P. D.; Calero, G.; Ackerson, C. J.; Bushnell, D. A.; Kornberg, R. D. Structure of a Thiol Monolayer-Protected Gold Nanoparticle at 1.1 Å Resolution. *Science* 2007, 318 (5849), 430–433.
- (6) Rai, M.; Yadav, A.; Gade, A. Silver Nanoparticles as a New Generation of Antimicrobials. *Biotechnol. Adv.* 2009, 27 (1), 76–83.
- (7) Standridge, S. D.; Schatz, G. C.; Hupp, J. T.; Standridge, S. D.; Schatz, G. C.; Hupp, J. T. Toward Plasmonic Solar Cells: Protection of Silver Nanoparticles via Atomic Layer Deposition of TiO₂. Langmuir 2009, 25 (5), 2596–2600.
- (8) Mcmahon, M. D.; Lopez, R.; Meyer, H. M.; Feldman, L. C.; Haglund, R. F. Rapid Tarnishing of Silver Nanoparticles in Ambient Laboratory Air. Appl. Phys. B Lasers Opt. 2005, 80 (7), 915–921.
- (9) Yang, J.; Jin, R. New Advances in Atomically Precise Silver Nanoclusters. ACS Mater. Lett. 2019, 1 (4), 482–489.
- (10) Bhattarai, B.; Zaker, Y.; Atnagulov, A.; Yoon, B.; Landman, U.; Bigioni, T. P. Chemistry and Structure of Silver Molecular Nanoparticles. Acc. Chem. Res. 2018, 51 (12), 3104–3113.
- (11) Yang, H.; Wang, Y.; Huang, H.; Gell, L.; Lehtovaara, L.; Malola, S.; Häkkinen, H.; Zheng, N. All-Thiol-Stabilized Ag44 and Au12Ag32 Nanoparticles with Single-Crystal Structures. Nat. Commun. 2013, 4, 2422.
- (12) Desireddy, A.; Conn, B. E.; Guo, J.; Yoon, B.; Barnett, R. N.; Monahan, B. M.; Kirschbaum, K.; Griffith, W. P.; Whetten, R. L.; Landman, U.; et al. Ultrastable Silver Nanoparticles. *Nature* 2013, 501, 399–402.
- (13) Conn, B. E.; Desireddy, A.; Atnagulov, A.; Wickramasinghe, S.; Bhattarai, B.; Yoon, B.; Barnett, R. N.; Abdollahian, Y.; Kim, Y. W.; Griffith, W. P.; et al. M 4 Ag 44 (p-MBA) 30 Molecular Nanoparticles. J. Phys. Chem. C 2015, 119 (20), 11238–11249.
- (14) Urushizaki, M.; Kitazawa, H.; Takano, S.; Takahata, R.; Yamazoe, S.; Tsukuda, T. Synthesis and Catalytic Application

- of Ag44 Clusters Supported on Mesoporous Carbon. *J. Phys. Chem. C* **2015**, *119*, 27483–27488.
- (15) Yoon, B.; Luedtke, W. D.; Barnett, R. N.; Gao, J.; Desireddy, A.; Conn, B. E.; Bigioni, T.; Landman, U. Hydrogen-Bonded Structure and Mechanical Chiral Response of a Silver Nanoparticle Superlattice. Nat. Mater. 2014, 13, 807–811.
- (16) Zeng, C.; Chen, Y.; Kirschbaum, K.; Lambright, K. J.; Jin, R. Emergence of Hierarchical Structural Complexities in Nanoparticles and Their Assembly. 2016, 354 (6319), 1580– 1585.
- (17) Conn, B. E.; Atnagulov, A.; Yoon, B.; Barnett, R. N.; Landman, U.; Bigioni, T. P. Confirmation of a de Novo Structure Prediction for an Atomically Precise Monolayer-Coated Silver Nanoparticle. Sci. Adv. 2016, 2, e1601609.
- (18) Wan, X.-K.; Wang, J.-Q.; Nan, Z.-A.; Wang, Q.-M. Ligand Effects in Catalysis by Atomically Precise Gold Nanoclusters. Sci. Adv. 2017, 3, e1701823.
- (19) Dufour, F.; Fresch, B.; Purupthy, O.; Cheneac, C.; Remacle, F. Ligand and Solvation Effects on the Structural and Electronic Properties of Small Gold Clusters. J. Phys. Chem. C 2014, 118, 4362–4376.
- (20) Kim, A.; Zeng, C.; Zhou, M.; Jin, R. Surface Engineering of Au36(SR)24 Nanoclusters for Photoluminescence Enhancement. Part. Part. Syst. Charact. 2017, 34 (8), 1600388.
- (21) Chevrier, D. M.; Raich, L.; Rovira, C.; Das, A.; Luo, Z.; Yao, Q.; Chatt, A.; Xie, J.; Jin, R.; Akola, J.; et al. Molecular-Scale Ligand Effects in Small Gold–Thiolate Nanoclusters. *J. Am. Chem. Soc.* **2018**, *140* (45), 15430–15436.
- (22) Newville, M.; Boyanov, B. I.; Sayers, D. E. Estimation of Uncertainties in XAFS Data. J. Synchrotron Radiat. 1999, 6, 264–265.
- (23) D.A. Case, I.Y. Ben-Shalom, S.R. Brozell, D.S. Cerutti, T.E. Cheatham, III, V.W.D. Cruzeiro, T.A. Darden, R.E. Duke, D. Ghoreishi, M.K. Gilson, H. Gohlke, A.W. Goetz, D. Greene, R Harris, N. Homeyer, S. Izadi, A. Kovalenko, T. Kurtzman, T.S. Lee, S. LeGra, D. M. Y. and P. A. K. AMBER 2018. University of California, San Francisco 2018.
- (24) Wang, J. M.; Wolf, R. M.; Caldwell, J. W.; Kollman, P. A.; Case, D. A. Development and Testing of a General Amber Force Field. J. Comput. Chem. 2004, 25, 1157.
- (25) Maier, J. A.; Martinez, C.; Kasavajhala, K.; Wickstrom, L.; Hauser, K. E.; Simmerling, C. Ff14SB: Improving the Accuracy of Protein Side Chain and Backbone Parameters from Ff99SB. J. Chem. Theory Comput. 2015, 11 (8), 3696–3713.
- (26) Jorgensen, W. L.; Chandrasekhar, J.; Madura, J. D.; Impey, R. W.; Klein, M. L. Comparison of Simple Potential Functions for Simulating Liquid Water. J. Chem. Phys. 1983, 79, 926.
- (27) Hutter, J.; Iannuzzi, M.; Schiffmann, F.; VandeVondele, J. Cp2k: Atomistic Simulations of Condensed Matter Systems. Wiley Interdiscip. Rev. Comput. Mol. Sci. 2014, 4 (1), 15–25.
- (28) Perdew, J.; Burke, K.; Ernzerhof, M. Generalized Gradient Approximation Made Simple. Phys. Rev. Lett. 1996, 77 (18), 3865–3868.
- (29) VandeVondele, J.; Hutter, J. Gaussian Basis Sets for Accurate Calculations on Molecular Systems in Gas and Condensed Phases. *J. Chem. Phys.* **2007**, *127* (11), 114105.
- (30) Goedecker, S.; Teter, M.; Hutter, J. Separable Dual-Space Gaussian Pseudopotentials. Phys. Rev. B 1996, 54 (3), 1703– 1710.
- (31) Hartwigsen, C.; Goedecker, S.; Hutter, J. Relativistic Separable Dual-Space Gaussian Pseudopotentials from H to Rn. *Phys. Rev. B* **1998**, *58* (7), 3641–3662.
- (32) Krack, M. Pseudopotentials for H to Kr Optimized for Gradient-Corrected Exchange-Correlation Functionals. *Theor. Chem. Acc.* **2005**, *114* (1), 145–152.
- (33) Grimme, S.; Antony, J.; Ehrlich, S.; Krieg, H. A Consistent and Accurate Ab Initio Parametrization of Density Functional Dispersion Correction (DFT-D) for the 94 Elements H-Pu. *J. Chem. Phys.* **2010**, *132* (15), 154104.
- (34) Laino, T.; Mohamed, F.; Laio, A.; Parrinello, M. An Efficient Real Space Multigrid QM/MM Electrostatic Coupling. *J. Chem. Theory Comput.* **2005**, *1* (6), 1176–1184.
- (35) Laino, T.; Mohamed, F.; Laio, A.; Parrinello, M. An Efficient

- Linear-Scaling Electrostatic Coupling for Treating Periodic Boundary Conditions in QM/MM Simulations. *J. Chem. Theory Comput.* **2006**, *2* (5), 1370–1378.
- (36) Genovese, L.; Deutsch, T.; Neelov, A.; Goedecker, S.; Beylkin, G. Efficient Solution of Poisson's Equation with Free Boundary Conditions. J. Chem. Phys. 2006, 125 (7), 74105.
- (37) Genovese, L.; Deutsch, T.; Goedecker, S. Efficient and Accurate Three-Dimensional Poisson Solver for Surface Problems. *J. Chem. Phys.* **2007**, *127* (5), 54704.
- (38) MacDonald, M. A.; Zhang, P.; Qian, H.; Jin, R. Site-Specific and Size-Dependent Bonding of Compositionally Precise Gold-Thiolate Nanoparticles from X-Ray Spectroscopy. *J. Phys. Chem. Lett.* **2010**, *1* (12), 1821–1825.
- (39) Glaser, T.; Hedman, B.; Hodgson, K. O.; Solomon, E. I. Ligand K-Edge X-Ray Absorption Spectroscopy: A Direct Probe of Ligand-Metal Covalency. Acc. Chem. Res. 2000, 33 (12), 859– 868.
- (TPB1) Bakr, O. M. et al. Silver nanoparticles with broad multiband linear optical absorption. Angew. Chem. Int. Edn 48, 5921–5926 (2009).
- (TPB2) W. D. Luedtke, U. Landman, Structure, dynamics, and thermodynamics of passivated gold nanocrystallites and their assemblies. J. Phys. Chem. 100, 13323–13329 (1996).
- (TPB3) "Synthetic and Post-Synthetic Chemistry of M₄Au_xAg_{44-x}(p-MBA)₃₀ Alloy Nanoparticles," Brian E. Conn, Badri Bhattarai, Aydar Atnagulov, Bokwon Yoon, Uzi Landman, and Terry P. Bigioni, *J. Phys. Chem. C* 122(24), 13166-13174 (2018).

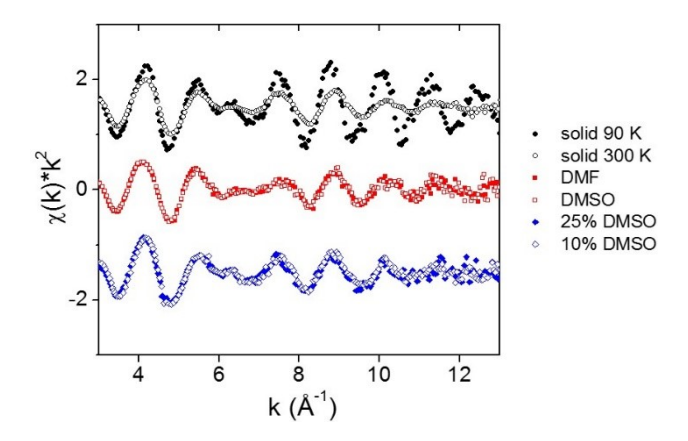


Figure S1. Ag K-edge k-space spectra of Na₄Ag₄₄(p-MBA)₃₀ NCs at various temperatures in the solid-phase and under solution-phase conditions.

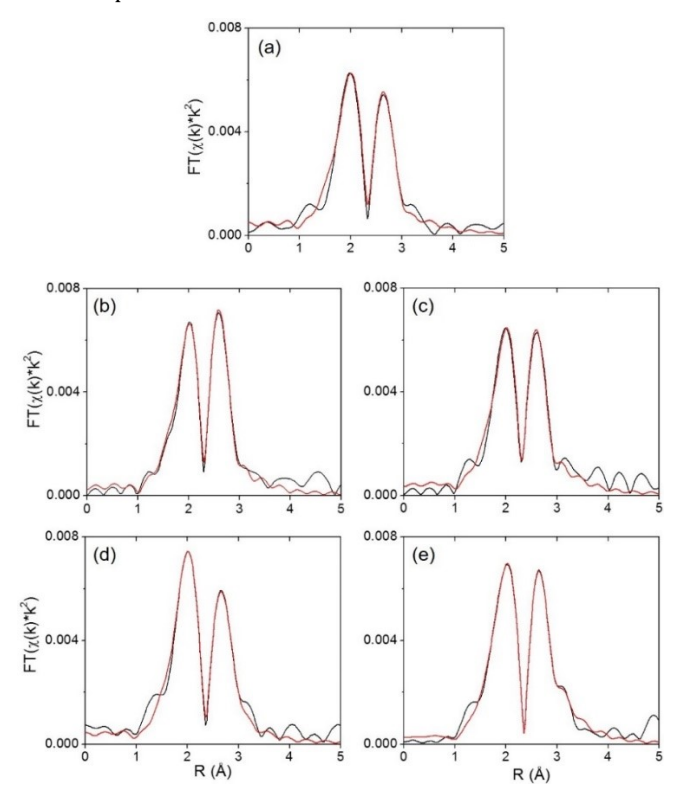


Figure S2. Ag K-edge EXAFS (black line) and multi-shell fit (red line) of $Na_4Ag_{44}(p\text{-}MBA)_{30}$ NCs in (a) solid-phase (300 K), (b) DMF, (c) DMSO, (d) 25% DMSO in water and (e) 10% DMSO in water.

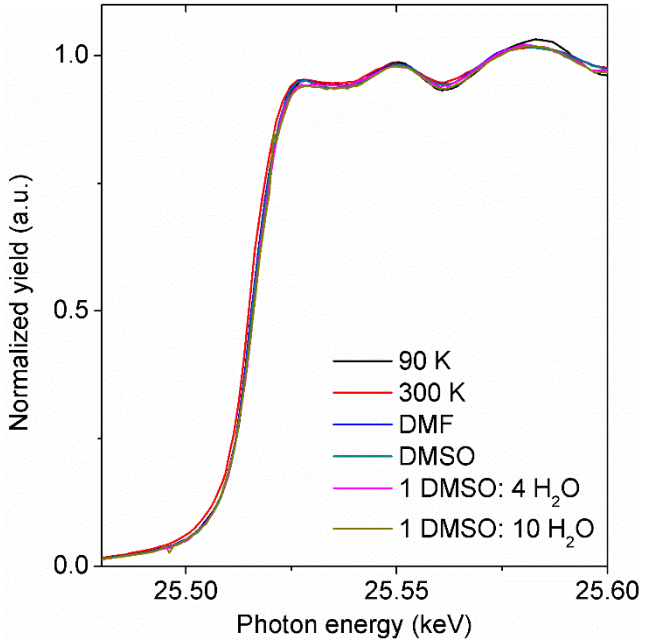


Figure S3. Ag K-edge XANES spectra of Na₄Ag₄₄(*p*-MBA)₃₀ NCs at various temperatures in the solid-phase and under solution-phase conditions.

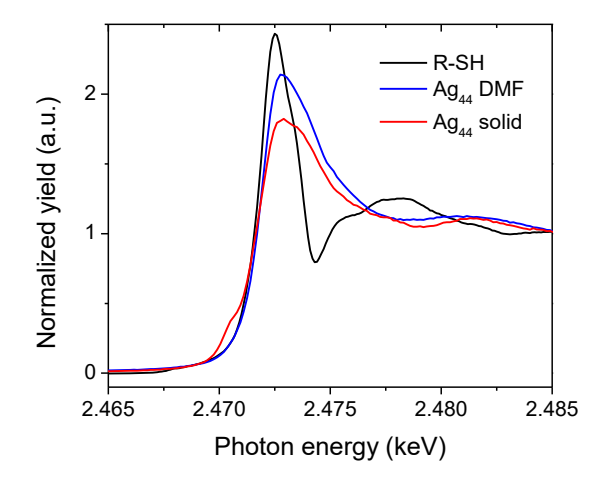


Figure S4. S K-edge XANES of free thiol (powder), $Na_4Ag_{44}(p-MBA)_{30}$ in DMF and $Na_4Ag_{44}(p-MBA)_{30}$ in solid form.

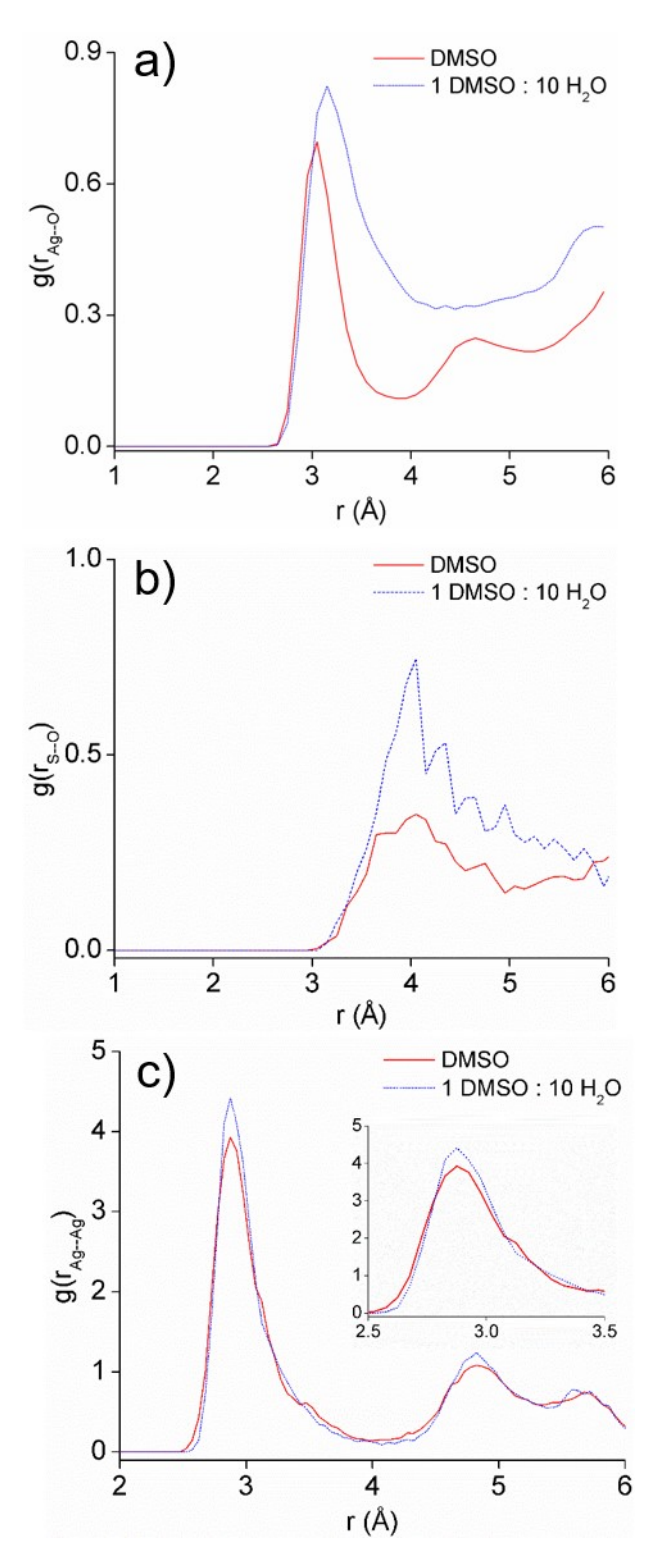


Figure S5. Radial distribution plots of a) sulfoxide distances to Ag atoms on NC surface, b) sulfoxide distances to S atoms of p-MBA ligands, c) Ag-Ag bond distances within Na₄Ag₄₄(*p*-MBA)₃₀.